The Response of Tropical Cyclone Statistics to an Increase in CO_2 with Fixed Sea Surface Temperatures

ISAAC M. HELD

NOAA/Geophysical Fluid Dynamics Laboratory, Princeton, New Jersey

MING ZHAO

NOAA/Geophysical Fluid Dynamics Laboratory, Princeton, New Jersey, and University Corporation for Atmospheric Research, Boulder, Colorado

(Manuscript received 24 January 2011, in final form 28 April 2011)

ABSTRACT

The effects on tropical cyclone statistics of doubling CO_2, with fixed sea surface temperatures (SSTs), are compared to the effects of a 2-K increase in SST, with fixed CO_2, using a 50-km resolution global atmospheric model. Confirming earlier results of Yoshimura and Sugi, a significant fraction of the reduction in globally averaged tropical storm frequency seen in simulations in which both SST and CO_2 are increased can be thought of as the effect of the CO_2 increase with fixed SSTs. Globally, the model produces a decrease in tropical cyclone frequency of about 10% due to doubling of CO_2 and an additional 10% for a 2-K increase in SST, resulting in roughly a 20% reduction when both effects are present. The relative contribution of the CO_2 effect to the total reduction is larger in the Northern than in the Southern Hemisphere. The average intensity of storms increases in the model with increasing SST, but intensity remains roughly unchanged, or decreases slightly, with the increase in CO_2 alone. As a result, when considering the frequency of more intense cyclones, the intensity increase tends to compensate for the reduced total cyclone numbers for the SST increase in isolation, but not for the CO_2 increase in isolation. Changes in genesis in these experiments roughly follow changes in mean vertical motion, reflecting changes in convective mass fluxes. Discussion of one possible perspective on how changes in the convective mass flux might alter genesis rates is provided.

1. Introduction

Most global high-resolution model simulations and downscaling studies project a reduction in the frequency of tropical cyclones, averaged over the globe, in response to global warming (e.g., Yoshimura et al. 2006; Bengtsson et al. 2007; Emanuel 2008; Gualdi et al. 2008; Sugi et al. 2009; Zhao et al. 2009), although there are a few exceptions showing little change globally (e.g., McDonald et al. 2005) or an increase (e.g., Wehner et al. 2010). [See Supplementary Material Table S1 in Knutson et al. (2010) for a summary.] It has been suggested by some that this intriguing response is connected, at least qualitatively, to a reduction in the tropically averaged deep convective mass flux (e.g., Sugi et al. 2002; Yoshimura et al. 2006; Bengtsson et al. 2007). This reduced convective mass flux can be rationalized, in turn, as a consequence of the larger projected fractional increase in the specific humidity, or more specifically, in the vertical gradient in humidity, as compared to a smaller projected increase in the mean precipitation as the climate warms (e.g., Betts 1998; Sugi and Yoshimura 2004; Held and Soden 2006; Vecchi and Soden 2007; O'Gorman and Schneider 2008). It has also been argued that a decrease in storm activity should result directly from the increase in the midtroposphere saturation deficit, the difference between the saturation and actual humidity (Emanuel et al. 2008). Also relevant are the radiative–convective simulations on an f plane of Nolan and Rappin (2008), which suggest that vertical shear becomes more effective at preventing genesis as temperatures increase.

A number of lines of evidence, ranging from global model results to downscaling studies to theories of potential intensity, suggest that an increase in intensity is also to be expected from global warming on average, if

Corresponding author address: Dr. Isaac M. Held, NOAA/Geophysical Fluid Dynamics Laboratory, Princeton University, Forrestal Campus, 201 Forrestal Rd., Princeton, NJ 08540–6649.
E-mail: isaac.held@noaa.gov

DOI: 10.1175/JCLI-D-11-00050.1

not in all regions. This increase in intensity can partially compensate or even overcompensate for the reduction in total cyclone number when considering changes in the number of very intense hurricanes and the destructive potential of storm activity (e.g., Emanuel 2008; Bender et al. 2010).

In some of the global modeling studies providing future projections for tropical cyclones, only the SSTs are changed, and the CO_2 concentration is not modified, assuming, in effect, that the dominant effect of increasing CO_2 on tropical cyclones is through the SST field. In other studies, both CO_2 and SSTs are increased, but the effects have not been broken down into the effect of increasing SST with fixed CO_2 and the effect of increasing CO_2 with fixed SSTs. In addition to helping us understand the response, this decomposition is relevant for discussions of geoengineering, such as Bala et al. (2010), in which one tries to counteract the effects of CO_2-induced warming on temperatures with a reduction in the absorbed solar flux, leaving behind the effects of the CO_2 increase in isolation.

The effect of an increase in CO_2 with fixed SSTs on aspects of global hydrology has been addressed in several papers (e.g., Sugi and Yoshimura 2004; Bala et al. 2010), but the only paper to our knowledge addressing the tropical cyclone problem in this context is that of Yoshimura and Sugi (2005) using a global model at T106 resolution. Yoshimura and Sugi (2005) find a significant decrease in cyclone frequency due to the effect of CO_2 in isolation—specifically a 13% decrease for doubling and $44\% = 2 \times 22\%$ for quadrupling. Their result has not received sufficient attention in our view, and our purpose here is to determine if the same qualitative response is present in the global model with which we have recently studied interannual variability, multidecadal trends, seasonal predictions, and projections for the future evolution of tropical storm statistics (Zhao et al. 2009, 2010; Zhao and Held (2010, hereafter ZH10). The future projections using this model have included simultaneous SST and CO_2 increases.

The following results are obtained from 4 integrations with a model identical to that utilized in Zhao et al. (2009). The first is a 25-yr control simulation with prescribed climatological (seasonally varying) SSTs and sea ice. This experiment is then perturbed in three ways: (i) by a uniform 2-K increase in all SSTs, (ii) by a doubling of the atmospheric CO_2, and (iii) by the simultaneous increase of 2 K and doubling of CO_2. The increase in SST of 2 K is roughly that expected from the transient climate response associated with a doubling of CO_2 (Randall et al. 2007). The perturbed runs are also all 25 yr long. The storm detection and tracking algorithm is described by Zhao et al. (2009). Tropical cyclones (TCs) are all warm-core vortices selected by this algorithm that have near-surface winds greater than 17 m s^{-1}. The term "hurricane" is used here in all basins for storms in which near-surface winds reach 33 m s^{-1}.

2. Results

The histograms in Fig. 1 show the fractional changes in the number of tropical cyclones (top panel) and hurricanes (bottom panel) in each of the three perturbation experiments (P2K = 2K increase in SST, $2 \times CO_2$, and both). The results are shown for the Northern and Southern Hemispheres separately as well as for the global mean. All experiments show decreases in TC counts in both hemispheres. Globally, the reductions are 11% for P2K, 10% for $2 \times CO_2$, and 21% for both. Our result is qualitatively similar to that of Yoshimura and Sugi (2005), for CO_2 in isolation, but somewhat smaller in magnitude. The 90% confidence interval is also shown for each result in the figure, assuming normal distributions and considering each year as an independent sample. If the upper limit of this interval is less than zero, then the reduction is significant at the 95% level. The reduction in TCs is estimated to be significant at 95% in all cases except for $2 \times CO_2$ in the Southern Hemisphere, which is marginal. The reduction in hurricanes is somewhat less significant because the coefficient of variation is roughly a factor of 2 larger for hurricanes than for all TCs. The sampling error from these 25-yr runs precludes addressing whether there is significant nonlinearity when one superposes the effects of doubling CO_2 and the SST increase. The computations with both effects present do provide evidence for a rough linearity and increase our confidence in the decomposition within this model.

There is also an indication that the relative contribution of the CO_2 increase to the reduction in TCs is larger in the Northern than in the Southern Hemisphere. A weaker response to the SST increase in the Northern than in the Southern Hemisphere and a stronger direct CO_2 response both contribute to this result. Longer integrations would be needed to make these distinctions more quantitative. One explanation for a larger response in the Northern Hemisphere would be that monsoonal responses associated with the warming of land are partly responsible for the reduction due to CO_2 in isolation, but we have no other evidence for this interpretation. We return to this issue briefly in section 3 below.

This figure also suggests that the relative contribution of CO_2 to the reduction in hurricanes tends to be greater than its contribution to the reduction in the frequency of all TCs. This is a consequence of the result, discussed more fully below, that the SST increase causes the

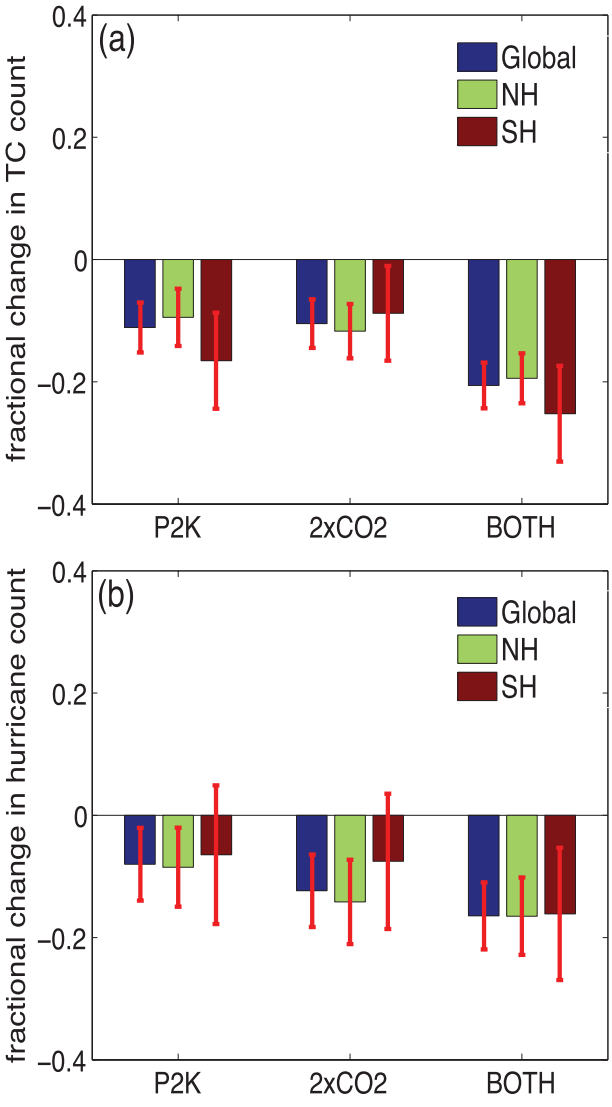

FIG. 1. (a) Fractional changes in annual TC count for the Northern Hemisphere (NH), the Southern Hemisphere (SH), and the globe (Global) between each perturbation experiment (P2K, $2 \times CO_2$, and both) and the control experiment. Error bars show the 90% confidence interval. (b) As in (a), but for hurricanes (storms with lifetime maximum near-surface winds exceeding 33 m s^{-1}).

average intensity to increase, while the CO_2 increase causes a slight reduction of intensity in this model.

Figure 2 shows the spatial pattern of the reduction in TC genesis in each of the three perturbation runs. Also shown in the figure for reference is the control simulation's distribution of genesis. [See Zhao et al. (2009) for a discussion of the climatological simulation.] These results are averaged over 4×5 (latitude–longitude) boxes and then filtered with a 9-point Gaussian filter to extract the signal more clearly from small-scale noise that is unlikely to be statistically significant. Both the P2K and $2 \times CO_2$ runs show reductions in most genesis regions. Both reduce the number of storms in the west Pacific, with $2 \times CO_2$ providing more of a reduction in genesis close to the East Asian coast. P2K results in a better-defined reduction in the southern Indian Ocean, while $2 \times CO_2$ and P2K have opposite effects in the east Pacific. Both show reductions in genesis through much of the tropical North Atlantic.

Several measures of intensity change in these simulations are included in Fig. 3. As described by ZH10 for the Atlantic basin, the distribution of intensities in this GCM is reasonable up to the hurricane threshold, after which the number of storms drops off too rapidly. ZH10 propose a simple statistical correction for this bias for the North Atlantic and test it against differences in intensity between active and inactive years. The difficulty in applying an analogous procedure to the global results presented here is that the required bias correction is basin dependent. In particular, the model storms in the North Pacific, while still weak on average, require less of a bias correction than do the North Atlantic storms. We have chosen to simply present the raw model intensities here.

We use the same notation for various intensity diagnostics as in ZH10. After computing the maximum wind speed at the lowest model level during each cyclone's lifetime, we then compute $F(I)$, the number of cyclones with this maximum lifetime intensity larger than a given value I. The change $\delta F(I)$, cyclones per year, from the control is displayed in the top panel of Fig. 3 for each of the three perturbation runs. The P2K run shows an increase in number of TCs with intensity greater than roughly 40 m s^{-1} despite the reduction in total number of TCs. The $2 \times CO_2$ run shows no transition of this type for higher intensity TCs. As a result, in the run with both effects present there is a smaller increase in frequency of the most intense cyclones in this model.

Setting $F = NP(I)$ where N is the total number of TCs, one can decompose the change in F into parts due to changes in N and changes in P. The middle panel in Fig. 3 shows $N\delta P(I)$, the contribution to δF due to changes in the intensity distribution. The value for N is taken from the control simulation. The distinction between the P2K and $2 \times CO_2$ perturbations is now more evident. The probability of a given TC exceeding the intensity I increases for all I in the P2K experiment and when both effects are present, but the $2 \times CO_2$ run, if anything, shows a small reduction in the probability of exceeding the hurricane threshold and higher intensities.

We also estimate the change in intensity as a function of intensity in the bottom panel in Fig. 3, following a procedure described in ZH10. From the two $P(I)$ curves for a perturbed and control simulation we first compute

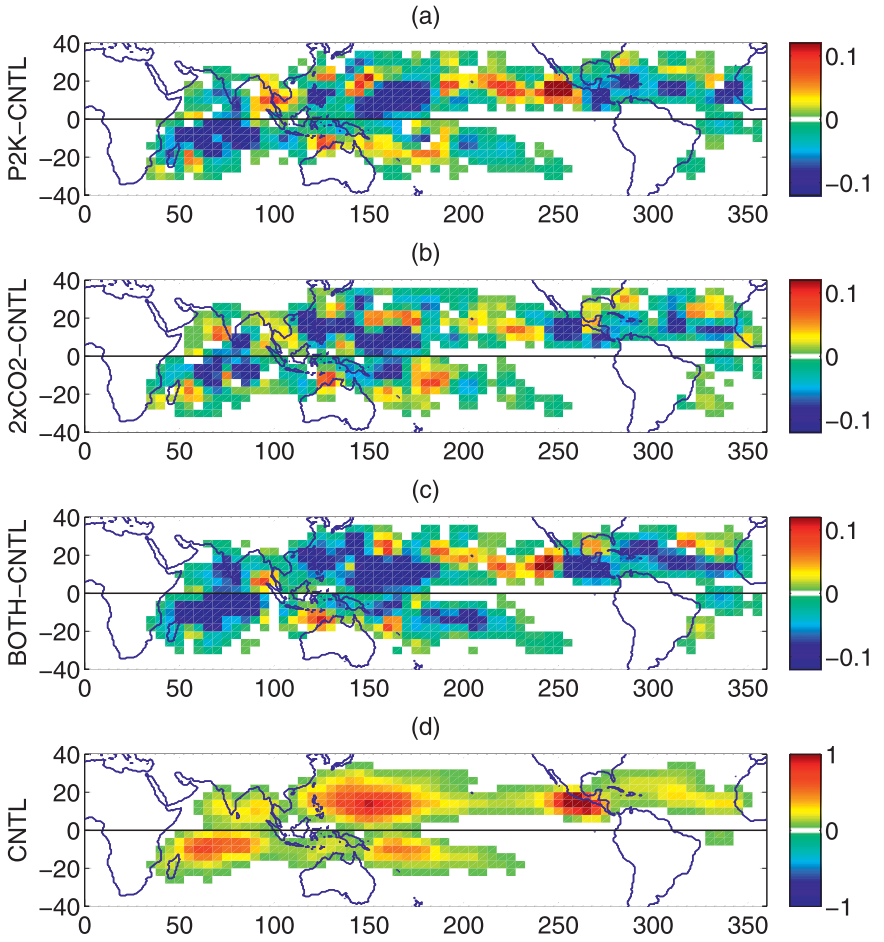

FIG. 2. Geographical distribution of the change in the frequency of genesis of TCs between each perturbation experiment and the control experiment: (a) P2K minus CNTL, (b) $2 \times CO_2$ minus CNTL, (c) both minus CNTL, (d) CNTL (unit: annual count per $4° \times 5°$ (latitude–longitude) area. Genesis is defined following the algorithm in Zhao et al. (2009), in terms of the first appearance of a warm-core vortex with surface wind speed greater than 17 m s^{-1} (the vortex must persist for at least 3 days).

δI at fixed P (rather than δP at fixed I as in the middle panel). But rather than plot δI versus P, we use the control $P(I)$ to convert from P to I, resulting in $\delta I(I)$. This procedure brings out the change in intensity at large I more clearly. Globally, the P2K experiment results in a small (less than 1 m s^{-1}) increase in intensity for $I < 40$ m s^{-1}, with the characteristic intensity increase rising to greater than 2 m s^{-1} for $I \approx 45$–50 m s^{-1}. The pattern is similar when both effects are present, while the CO_2 increase in isolation has a slight negative effect on intensity at nearly all intensity levels. These quantitative results are not to be taken at face value, as discussed in ZH10. But despite the model's intensity biases, these qualitative results suggest that intensity changes are mostly due to SSTs and not changes in CO_2, when the effects of these two are examined in isolation.

3. Some relationships between genesis and large-scale fields

The direct response of precipitation, both globally and regionally, to the change in CO_2 has been discussed, for example, by Sugi and Yoshimura (2004), Bala et al. (2010), and Andrews et al. (2010). In the present model the global response in precipitation is an increase of 6.8% for P2K, a reduction of 2.3% for $2 \times CO_2$, and a 4.2% increase for both together. To focus on those regions of most relevance to the present analysis, we define an average in which the quantity of interest, given as spatial maps of monthly means $[A(x, y, m), m = 1, 12]$, is weighted by the control simulation's spatial pattern of genesis $G(x, y, m)$, the annual mean of which is shown in Fig. 2:

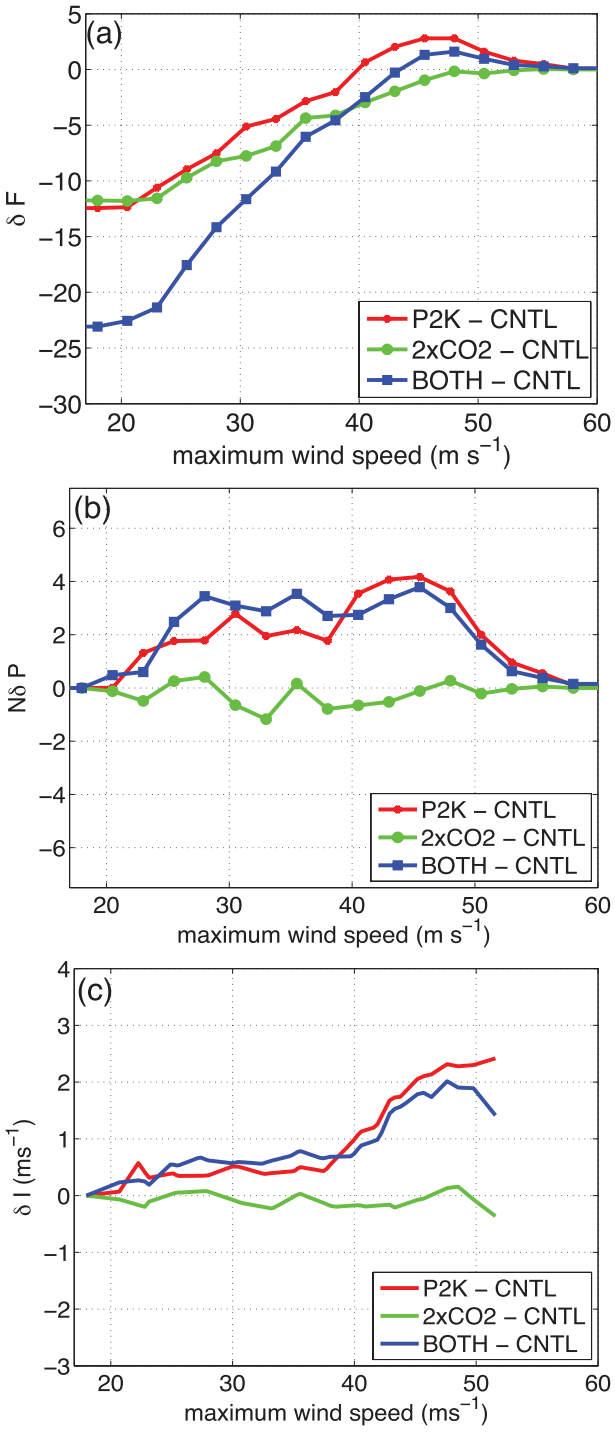

FIG. 3. (a) Changes $[\delta F(I)]$ in the (cumulative) frequency of TCs (number per year) with lifetime maximum wind speed exceeding each value of intensity I = lifetime maximum wind speed, computed over the global tropical ocean. (b) As in (a), but for the component of δF due to changes in cumulative probability distribution of intensity ($N\delta P$), where N is the total number of TCs per year. (c) As in (a), but for changes in intensity $[\delta I(I)]$. See text for the definition of notation.

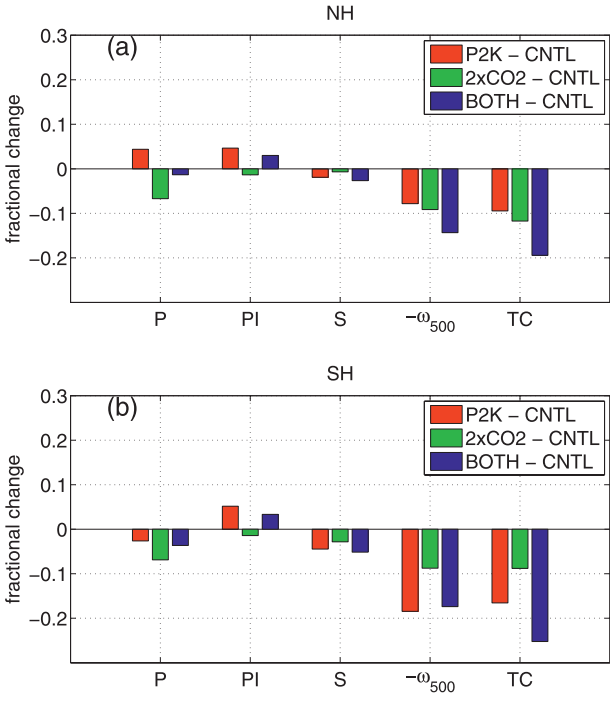

FIG. 4. Fractional change of mean precipitation (P), potential intensity (PI), an environmental shear index (S), 500-hPa mean ascent ($-\omega_{500}$), and mean TC genesis frequency (TC) over the Northern Hemisphere between each perturbation experiment and the control experiment. Here P, PI, S, and ω_{500} are weighted averages using the climatological TC genesis frequency distribution from the control simulation as the weighting function [see text and Eq. (1)]. (b) As in (a), but for the Southern Hemisphere.

$$\langle A\rangle_G \equiv \frac{\overline{GA}}{\overline{G}} \,. \tag{1}$$

The overline indicates an annual as well as spatial mean. The fractional changes in the genesis-weighted precipitation, $\langle \delta P\rangle_G/\langle P\rangle_G$, are displayed in Fig. 4, using separate spatial means over the two hemispheres. The precipitation changes remain of opposite sign for P2K and 2 × CO_2 in the Northern Hemisphere, although in contrast to the unweighted global mean, there is now a small decrease in the Southern Hemisphere in the P2K simulation. These precipitation changes are small and do not seem to be closely related to the much larger percentage changes in tropical storm genesis.

Also shown in Fig. 4 are similarly weighted hemispheric changes in potential intensity (PI), a shear index (S), and the negative of the pressure velocity ω at 500 hPa. Potential intensity (Emanuel 1988) is sometimes considered relevant for genesis and not only for storm intensity. For example, in the empirical model of Emanuel and Nolan (2004) and Camargo et al. (2007), genesis frequency is assumed proportional to the potential intensity raised to the third power. Genesis-weighted

averages are similar in both hemispheres, with a global average of $\langle \delta \mathrm{PI} \rangle_G = +2.5$ m s^{-1} for P2K, -0.7 m s^{-1} for $2 \times CO_2$, and, consistently, $+1.6$ m s^{-1} for both simultaneously. There is a rough consistency with the simulated intensity changes described above. [These values are computed following Bister and Emanuel (2002), assuming a ratio of thermal to momentum drag coefficients of 0.5 (consistent with the GCM formulation at hurricane intensities) and by assuming air parcel ascent between the pseudoadiabatic and adiabatic limits (SIG = 0.5 in ftp://texmex.mit.edu/pub/emanuel/TCMAX/). Storm dissipative heating is included in the calculation consistent with the inclusion of dissipative heating in the model's boundary layer parameterization.] Changes in PI clearly cannot be thought of as the dominant factor controlling changes in genesis, since the changes in PI are of opposite sign for the SST and CO_2 simulations while genesis decreases in both cases.

We define a vertical shear index (S) as the absolute value of the vector wind difference between 850 and 200 hPa, using monthly mean winds. The genesis weighted tropical average, $\langle S \rangle_G$ is reduced by roughly 1.3%–3.5% among the experiments, with larger reductions in the Southern Hemisphere, as shown in Fig. 4. Not only are these changes of the wrong sign to explain the reduction in genesis in the most naive way, they are very small. It is certainly possible that this gross shear index is not a good way of summarizing the effects of large-scale circulation changes on genesis.

If one computes the genesis-weighted change in monthly mean ω at 500 hPa, $\langle \delta\omega_{500} \rangle_G / \langle \omega_{500} \rangle_G$, as a simple measure of tropical deep convective activity,[1] one obtains the fractional changes shown in Fig. 4. There is a reduction in deep convective activity in both hemispheres, with substantially weaker upward motion, consistent with the physical arguments and model results discussed by Knutson and Manabe (1995), Betts (1998), Sugi and Yoshimura (2004), Held and Soden (2006), and O'Gorman and Schneider (2008). For convenience, Fig. 4 also replots the fractional changes in tropical cyclone frequency in the two hemispheres shown in Fig. 1. Not only the sign, but the relative magnitude of the effects in P2K and $2 \times CO_2$, and in the two hemispheres, are now qualitatively consistent, suggesting the plausibility of a causal connection between changes in overall convective activity in regions of genesis and changes in tropical cyclone frequency.

To examine the spatial structure of the changes in these potentially relevant large-scale indices, we compute each index, for each 4×5 (latitude–longitude) grid square, weighting the 12 months by the control model's genesis rate for that month:

$$[A(x, y)]_G \equiv \frac{\widetilde{G(x,y)A(x,y)}}{\widetilde{G(x,y)}}, \tag{2}$$

where the tilde is an average over the 12 months. The genesis weighting provides a compact way of defining a map of the change in the index at the most relevant times of year.

Figure 5 contains maps of $[\delta\omega_{500}]_G$ for the three simulations. There is some similarity between this map and that of the change in genesis frequency, with a reduction in most genesis regions in both the $2 \times CO_2$ and P2K cases, the clearest exception being in the east Pacific in P2K, where there is an increase in genesis and a somewhat noisy increase in mean upward motion. The fractional contribution of TCs themselves to the mean upward motion should be comparable to their fractional contribution to precipitation, and estimates of the latter (Jiang and Zipser 2010) indicate that this fraction is small in nearly all of the major genesis regions. We have confirmed that this is the case in our GCM as well. The resemblance of the change in genesis-weighted upward motion to the change in TC frequency suggests that TC genesis is being influenced by the same factors that influence the more pervasive less-organized component of deep convection.

From the maps of the local $[\delta \mathrm{PI}]_G$ in Fig. 6 we learn that these changes are relatively uniform in these simulations. The changes in the intensity of the model's storms, as documented in Fig. 3, are qualitatively consistent with these PI changes, averaged over the tropics. While the $2 \times CO_2$ simulation in isolation might be suggestive of a connection between storm frequency and PI, the P2K simulation is inconsistent with this effect being dominant, as discussed earlier.

These changes in PI are dominated by changes in the atmosphere–ocean disequilibrium in enthalpy, which decreases in most of the tropics in the $2 \times CO_2$ case and

[1] Typically, over the tropical oceans in regions of mean upward motion, the precipitation greatly exceeds evaporation. Thinking of a simple moisture budget for such a region, the column-integrated convergence of vapor can be thought of as qw, where q is the difference in humidity between the boundary layer and free troposphere, and w the upward mean flow at the top of the moist layer. The time-averaged column-integrated moisture budget is then $qw \approx P - E$ = precipitation minus evaporation, while the moisture budget of the free troposphere is $qM = P$, where M is the mass exchanged between the moist lower layer and the drier free troposphere. Thus, the mean w is an approximate surrogate for M to the extent that E is small compared with P. Examining the convective mass flux produced by the model's parameterization scheme is not a good measure of M in this model, since a substantial fraction of tropical precipitation occurs in the model's "large scale" component.

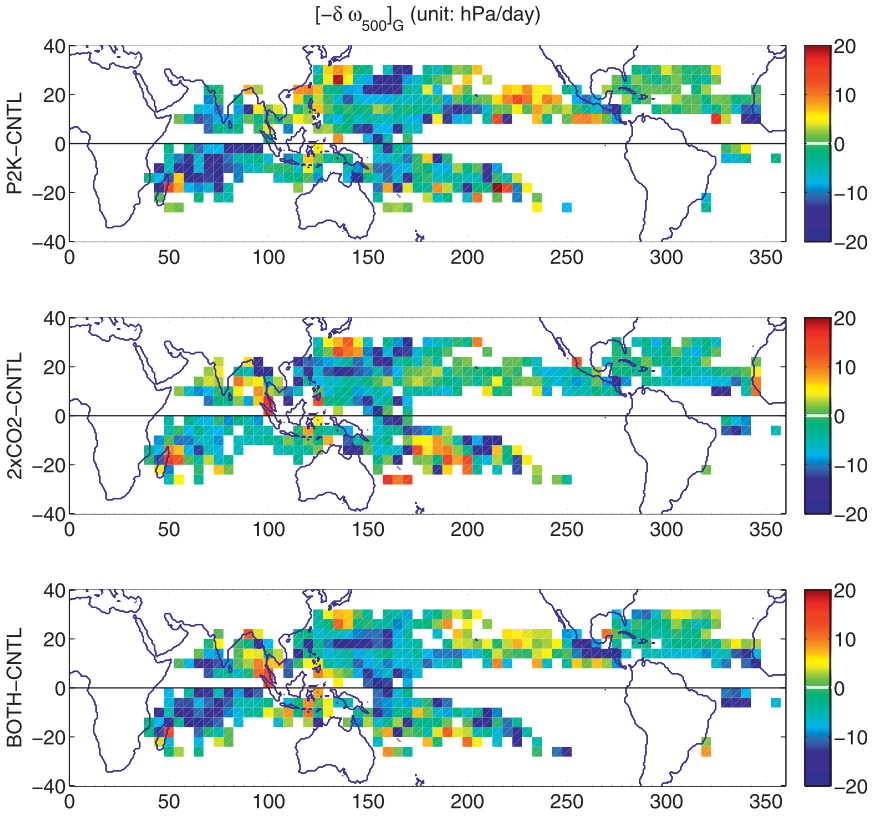

FIG. 5. Geographical distribution of the change in 500-hPa vertical velocity weighted by TC genesis frequency ($[-\delta\omega_{500}]_G$) as described in Eq. (2) between each perturbation experiment and the control experiment. (top) P2K minus CNTL, (middle) 2 × CO_2 minus CNTL, and (bottom) both minus CNTL.

increases in P2K (Emanuel 2007). The changes in the enthalpy jump near the surface in turn are of the same sign as the tropical mean changes in evaporation (or precipitation)—an increase for P2K and a decrease for 2 × CO_2. Changes in surface winds are of secondary importance; on average, the near-surface relative humidity adjusts to produce the changes in evaporation/precipitation demanded by the atmospheric energy budget. Changes to free-tropospheric moisture and temperature are very small in the 2 × CO_2 case.

In Fig. 7, we plot the spatial structure of the change in $[\delta S]_G$. There is no obvious correspondence between these patterns and changes in genesis (spatial correlations are close to zero). If changes in circulation are important, their effect is not captured by this simple large-scale, monthly mean shear index. We have not tried other possibilities, such as a change in the Doppler-shifted phase speed of easterly waves, as suggested by the ''pouch'' perspective of Dunkerton et al. (2009) or changes conducive to poleward propagation of easterly wave trains (e.g., Dickinson and Molinari 2002; Li 2006). While inspection of the large-scale flow indicates that there are changes in monsoonal circulations in the 2 × CO_2 simulation, neither the spatial structure in S nor in the genesis itself suggest that these changes are responsible for the bulk of the reduction in genesis.

Rather than using spatial structures to try to infer relationships between changes in genesis and changes in large-scale indices, such as monthly mean ω, PI, or S, one can follow the analysis of cloud feedbacks in Bony et al. (2004), and think instead of the probability of genesis, given a value of the index, irrespective of location. That is, one writes the total genesis as $\int g(\xi)P(\xi)\,d\xi$, where ξ is some large-scale index, $P(\xi)\,d\xi$ is the probability of ξ lying within $(\xi, \xi + d\xi)$, $g(\xi)P(\xi)\,d\xi$ is the number of cyclones forming with ξ in this range, and $g(\xi)$ is mean cyclone genesis frequency at given ξ. One can then decompose the change in gP as $\delta(gP) \approx g\delta P + P\delta g + \delta P\delta g$. Table 1 shows this decomposition, integrated over ξ, for the three different perturbation experiments. While the quadratic terms is not always small, especially in the P2K case for ξ = PI, it is never large enough to change the fundamental picture. In the limit that ξ is an irrelevant variable, the term $g\delta P$ should vanish when integrated

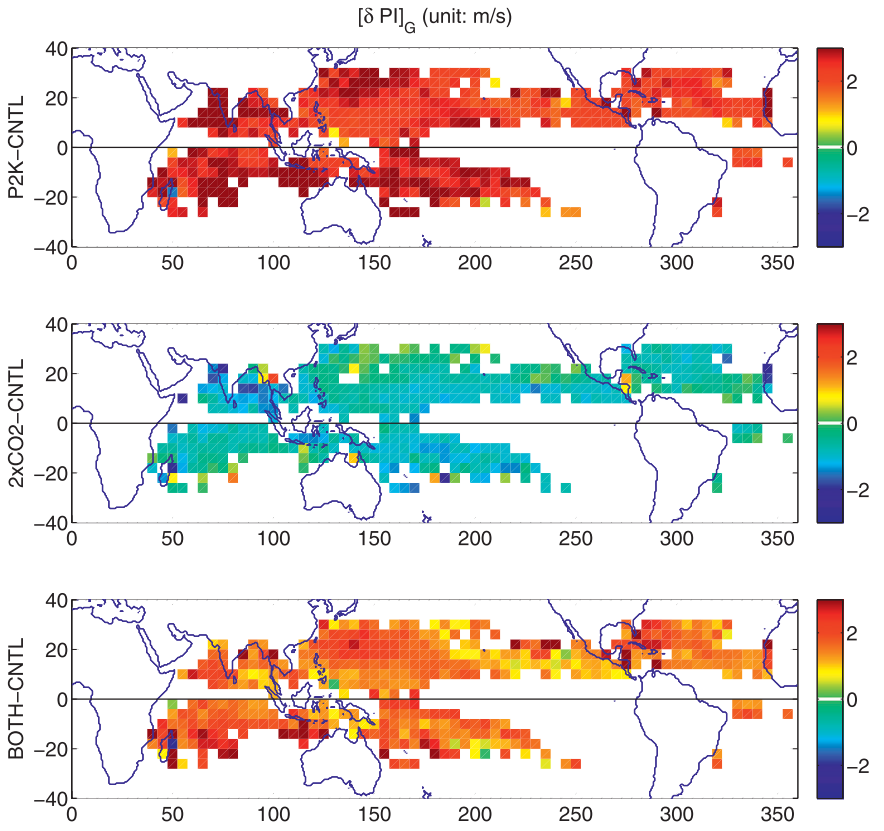

FIG. 6. As in Fig. 5, but for potential intensity.

over ξ, and $P\delta g$ should explain the total signal. In the opposite extreme, in which g is simply a function of ξ, the probability of genesis, given ξ, should not change, and the term $g\delta P$ should dominate.

As shown in Table 1, the integrated contribution due to $g\delta P$ is small for both $\xi = S$ and $\xi = \mathrm{PI}$, whether one is perturbing CO_2, SST, or both. For the shear index, the integrated change due to $g\delta P$ is actually of the opposite sign to the net change. This is consistent with the claim that perturbations in neither variable exert a dominant influence on genesis in this model. In contrast, for $\xi = \omega_{500}$, $g\delta P$ contributes roughly 50% of the reduction in genesis for the three perturbations.

Figure 8 shows this decomposition in more detail, as a function of ξ. The top panel is gP in the control simulation, while the middle and bottom panels are $g\delta P$ and $P\delta g$, respectively. The top panel shows that genesis predominately occurs only when $40 < \mathrm{PI} < 60$ m s^{-1}, $S < 15$ m s^{-1}, and $-150 < \omega_{500} < 0$ (hPa day^{-1}), all indices being monthly means.

For $\xi = \mathrm{PI}$, the results conform to expectations if the shift in the distribution of PI, toward larger values for P2K and smaller values for CO_2, have little effect on genesis in the model. For the shear index S, there is an increase in the frequency of very low values when SSTs are increased, and this generates the small positive $g\delta P$ term seen in Table 1. But the bottom panel ($P\delta g$) indicates a reduction in genesis at all shears, more or less proportional to the unperturbed distribution. For $\xi = \omega_{500}$, in both the increased SST and CO_2 cases, there is a reduction in frequency in values of ω_{500} between -50 and -150 hPa day^{-1}, compensated by an increase in frequency of weaker mean uplift, but, when weighted by the likelihood of genesis in the control model the effects of the reduction in frequency of stronger uplift dominate. There are also some reductions in genesis associated with the rate of genesis at fixed ω, arguing that there are other controlling factors. But for the three indices examined, the results for ω_{500} are the only ones that suggest an explanation for the genesis reduction.

Our hypothesis is that changes in storm frequency in these simulations are primarily controlled by the overall amount of deep convective activity in regions that are otherwise favorable for genesis.

4. Comments on the connection between convective mass fluxes and genesis

A theory for genesis roughly consistent with these results might take the form $G = M\mathcal{G}(p, q, \ldots)$, where M

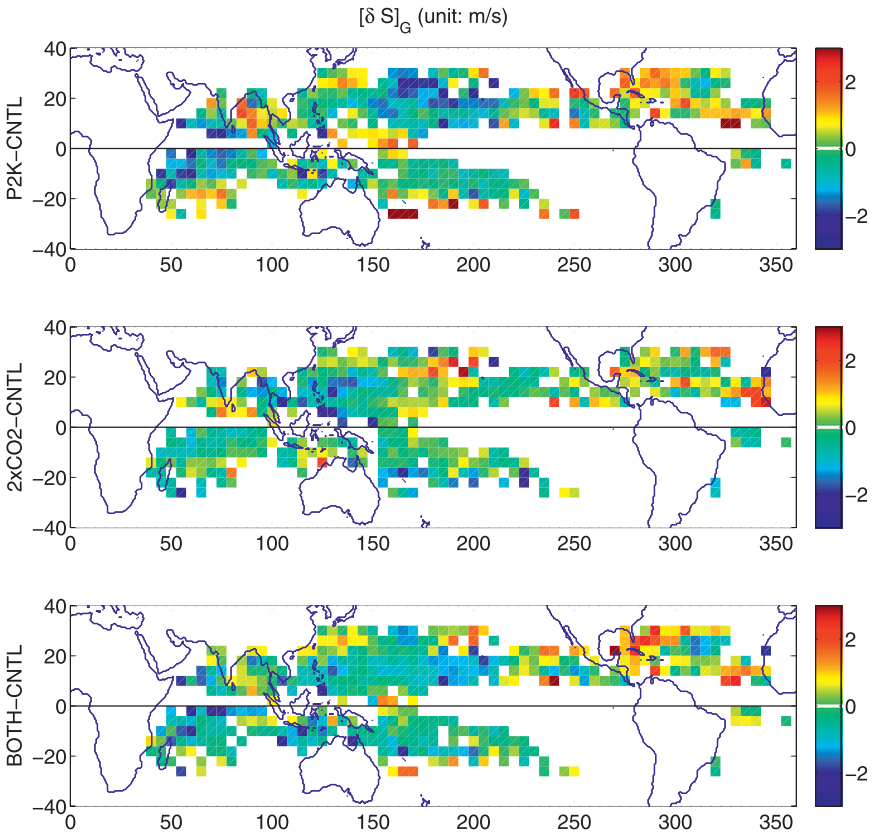

FIG. 7. As in Fig. 5, but for vertical wind shear defined as the absolute value of the vector wind difference between 850 and 200 hPa using monthly mean winds.

is the total convective mass flux, while p, q, … are environmental indices that affect the manner in which this raw material M is organized. As an example of the kind of argument consistent with this perspective, we provide a qualitative discussion of the roles of the convective mass flux, shear, and midtropospheric environmental moisture in the generation of a moist midtroposphere conducive for genesis.

Focusing on the successful moistening of the midtroposphere as a central element in genesis is consistent with proposed genesis indices (DeMaria et al. 2001), field program such as the Tropical Experiment in Mexico (TEXMEX; Bister and Emanuel 1997), idealized models (Rotunno and Emanuel 1987), and the recent "pouch" perspective (Dunkerton et al. 2009), which can be thought of, in part, as diagnosing situations in which the region being moistened by convection is protected from mixing with drier environmental air. The following discussion is also motivated by the study of genesis in a radiative–convective model with imposed shear in Nolan et al. (2007) and Nolan and Rappin (2008).

For this purpose, we write the specific humidity balance in the midtroposphere as

$$U\frac{\partial q_m}{\partial x} \sim (M_c - w)\frac{\partial q_m}{\partial z} + D(q_c - q_m). \qquad (3)$$

On the right-hand side, M_c is the convective updraft volume flux; w is total vertical velocity, so that $M_c - w$

TABLE 1. Decomposition of the total change in gP into the three components: $g\delta P$, $P\delta g$, and $\delta g\delta P$ between each perturbation experiment and the control experiment. All terms are integrated over $\xi(\xi = \omega_{500}, S, \text{PI})$ and are shown with percentage changes.

	P2K − CNTL	2 × CO_2 − CNTL	BOTH − CNTL
Tot	−11.0%	−10.2%	−20.7%
$\xi = \omega_{500}$			
$g\delta P$	−5.9%	−4.9%	−9.6%
$P\delta g$	−4.9%	−5.8%	−11.6%
$\delta g\delta P$	−0.3%	+0.5%	+0.4%
$\xi = S$			
$g\delta P$	+2.3%	+0.6%	+3.0%
$P\delta g$	−13.2%	−10.7%	−23.2%
$\delta g\delta P$	−0.2%	−0.0%	−0.5%
ξ = PI			
$g\delta P$	+2.2%	−0.7%	+4.0%
$P\delta g$	−19.3%	−10.4%	−25.9%
$\delta g\delta P$	+6.0%	+0.9%	+1.3%

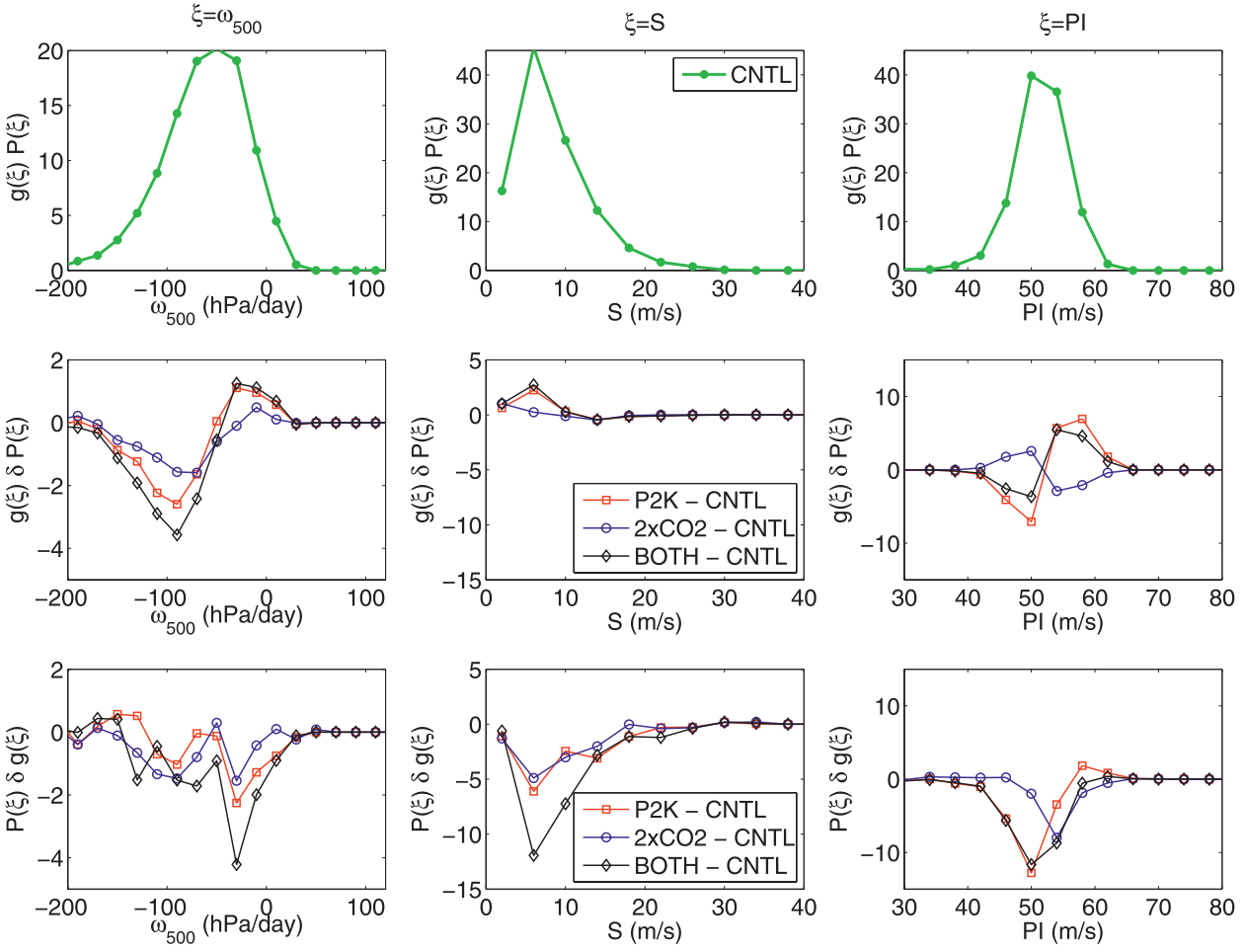

FIG. 8. (top) $g(\xi)P(\xi)$ from the control simulation, (middle) $g(\xi)\delta P(\xi)$ from each perturbation experiment and the control experiment, and (bottom) as in (middle), but for $P(\xi)\delta g(\xi)$. (left) $\xi = \omega_{500}$, (middle) ξ = shear, and (right) ξ = potential intensity. [See text for the definition of $g(\xi)$ and $P(\xi)$.]

represents the downward vertical velocity of environmental air outside the convective updraft; D is the detrainment rate from convective cores into the environment; while q_c and q_m are, respectively, the in-cloud total water and environmental specific humidity at some representative midtropospheric level. The left-hand side can be thought of as standing in for a variety of horizontal advective processes on various length scales. The strength of vertical shear can be thought of as proportional to U.

There are two limiting cases of interest: a region in which precipitation is much larger than evaporation on average, in which M_c and w roughly cancel, and radiative–convective equilibrium, in which $w = 0$. We focus on the first of these simplifications as being especially relevant for regions in which genesis typically occurs. The balance is now between drying due to the import of environmental air and moistening due to detrainment. Assuming that the detrainment is proportional to the cloud-base mass flux, M_b, and that $\partial q_m/\partial x \sim q_m/L$, and ignoring changes in horizontal length scale L, we then have

$$\frac{\delta U}{U} \sim \frac{\delta M_b}{M_b} + \frac{\delta \gamma}{\gamma}, \tag{4}$$

where $\gamma \equiv (q_c - q_m)/q_m$. Thought of as an expression for δU, Eq. (4) estimates how shears would need to change for their drying tendency to balance changes in the moistening tendencies. If δU is negative, the implication is that smaller advective drying tendencies are needed to overcome typical convective moistening tendencies, so that weaker "shears" are able to suppress genesis. Genesis would then be expected to decrease if the spectrum of advective drying tendencies is, in fact, unchanged.

One can consider two limiting cases for the in-cloud water: reversible ascent with in-cloud water equal to the humidity in the boundary layer, $q_c = q_b$, and pseudoadiabatic ascent with all condensate dropping out as it is formed, $q_c = q^*(T_m)$, where q^* is the saturation specific humidity. Reality and the GCM are both intermediate between these two extremes. For the pseudoadiabatic case, if relative humidities are assumed to remain unchanged, then $\delta\gamma \approx 0$ and $\delta U/U \sim \delta M_b/M_b$. In the case of reversible ascent, $\delta\gamma/\gamma$ should be negative as the temperatures increase, since fractional changes in q_m are expected to be larger than the fractional changes in $q_b - q_m$ if relative humidities remain unchanged and if the temperature profile remains close to a moist adiabat.

For the case of a CO_2 increase with fixed SSTs, changes in atmospheric moisture are small and, irrespective of the choice of adiabat used to estimate cloud water, the result of this crude scaling is $\delta U/U \sim \delta M_b/M_b$. For the SST increase, according to these estimates moisture changes would likely amplify the reduction in δU somewhat, or decrease genesis, over the expected decrease from δM in isolation.

The picture underlying this scaling is simply that decreased mass flux makes it easier for advection of dry air to suppress genesis.

5. Conclusions

This work is a continuation of a series of studies in which a global atmospheric model of roughly 50-km resolution is used to study aspects of the statistics of tropical cyclogenesis. (Zhao et al. 2009, 2010; ZH10). A reduction in tropical mean cyclogenesis is simulated by this model when subjected simultaneously to the patterns of SST change generated by a variety of coupled climate models and to a CO_2 increase. In this paper we separate the effects of the SST change (idealized as a 2-K uniform warming) and the increase (a doubling) in CO_2.

In this model the roughly 20% reduction is due, in roughly equal proportions, to the increase in SSTs with fixed CO_2 and to the increase in CO_2 with fixed SST, qualitatively confirming earlier results of Yoshimura and Sugi (2005). Analysis of these integrations suggests that the reduction of the convective mass flux, which occurs in both simulations, underlies this reduction in genesis. A crude scaling is provided that suggests that one can rationalize this dependence on convective mass flux by focusing on the competition between moistening of the midtroposphere by convection and the drying by horizontal advection.

While the model-generated storm intensities cannot be considered quantitatively useful in general, this model does produce a realistic distribution of intensities at least up to hurricane strength (ZH10). The model increases intensities when SSTs are increased by 2 K, and decreases intensities only slightly when CO_2 is doubled. The result is that the relative suppression of hurricanes as compared to all tropical cyclones is stronger for the CO_2 increase than for the SST increase, averaged over the tropics.

We emphasize that the tropical mean reduction in genesis discussed here should be differentiated from the changes in particular regions such as the North Atlantic. Regional changes in this model differ substantially from these results when the changes in SST are not spatially uniform but instead reflect the changes in the spatial pattern of warming projected by coupled GCMs (Zhao et al. 2009; ZH10).

Acknowledgments. We thank Tom Knutson, Gabriel Vecchi, Steve Garner, and Kevin Walsh for their helpful discussions on this topic, and S.-J. Lin for his central role in the development of this model. We also thank Kerry Emanuel, David Nolan, and Tim Merlis for their helpful comments on a previous draft. This research used resources of the National Center for Computational Sciences at Oak Ridge National Laboratory, which is supported by the Office of Science of the Department of Energy under Contract DE-AC05-00OR22725. An award of computer time was provided by the Innovative and Novel Computational Impact on Theory and Experiment Program. Ming Zhao was supported in part by NSF Grant ATM-0612551 and in part under Award NA17RJ2612 from the National Oceanic and Atmospheric Administration, U.S. Department of Commerce. The findings are those of the authors and do not necessarily reflect the views of the National Oceanic and Atmospheric Administration, or the U.S. Department of Commerce.

REFERENCES

Andrews, T., P. M. Forster, O. Boucher, N. Bellouin, and A. Jones, 2010: Precipitation, radiative forcing and global temperature change. *Geophys. Res. Lett.,* **37,** L14701, doi:10.1029/2010GL043991.

Bala, G., K. Caldeira, and R. Nemani, 2010: Fast versus slow response in climate change: Implications for the global hydrological cycle. *Climate Dyn.,* **35,** 423–434, doi:10.1007/s00382-009-0583-y.

Bender, M., T. Knutson, R. Tuleya, J. Sirutis, G. Vecchi, S. T. Garner, and I. Held, 2010: Modeled impact of anthropogenic warming on the frequency of intense Atlantic hurricanes. *Science,* **327,** 454–458.

Bengtsson, L., K. Hodges, M. Esch, N. Keenlyside, L. Kornblueh, J.-J. Luo, and T. Yamagata, 2007: How may tropical cyclones change in a warmer climate. *Tellus,* **59A,** 539–561.

Betts, A. K., 1998: Climate-convection feedbacks: Some further issues. *Climate Change,* **39,** 35–38.

Bister, M., and K. A. Emanuel, 1997: The genesis of hurricane Guillermo: TEXMEX analyses and a modeling study. *Mon. Wea. Rev.,* **125,** 2662–2682.

——, and ——, 2002: Low frequency variability of tropical cyclone potential intensity 1. Interannual to interdecadal variability. *J. Geophys. Res.,* **107,** 4801, doi:10.1029/2001JD000776.

Bony, S., J.-L. Dufresne, H. L. Treut, J.-J. Morcrette, and C. Senior, 2004: On dynamic and thermodynamic components of cloud changes. *Climate Dyn.,* **22,** 71–86.

Camargo, S., A. Sobel, A. G. Barnston, and K. Emanuel, 2007: Tropical cyclone genesis potential index in climate models. *Tellus,* **59A,** 428–443.

DeMaria, M., J. Knaff, and B. H. Connell, 2001: A tropical cyclone genesis parameter for the tropical Atlantic. *Wea. Forecasting,* **16,** 219–233.

Dickinson, M., and J. Molinari, 2002: Mixed Rossby–gravity waves and western Pacific tropical cyclogenesis. Part I: Synoptic evolution. *J. Atmos. Sci.,* **59,** 2183–2196.

Dunkerton, T., M. Montgomery, and Z. Wang, 2009: Tropical cycloegenesis in a tropical wave critical layer: Easterly waves. *Atmos. Chem. Phys.,* **9,** 5587–5646.

Emanuel, K., 1988: The maximum intensity of hurricanes. *J. Atmos. Sci.,* **45,** 1143–1155.

——, 2007: Environmental factors affecting tropical cyclone power dissipation. *J. Climate,* **20,** 5497–5509.

——, 2008: The hurricanes–climate connection. *Bull. Amer. Meteor. Soc.,* **89,** ES10–ES20.

——, and D. Nolan, 2004: Tropical cyclones and the global climate system. Extended Abstracts, *26th AMS Conf. on Hurricanes and Tropical Meteorology,* Miami, FL, Amer. Meteor. Soc., 10A.1. [Available online at http://ams.confex.com/ams/pdfpapers/75463.pdf.]

——, R. Sundararajan, and J. Williams, 2008: Hurricanes and global warming: Results from downscaling IPCC AR4 simulations. *Bull. Amer. Meteor. Soc.,* **89,** 347–367.

Gualdi, S., E. Scoccimarro, and A. Navarra, 2008: Changes in tropical cyclone activity due to global warming: Results from a high-resolution coupled general circulation model. *J. Climate,* **21,** 5204–5228.

Held, I. M., and B. J. Soden, 2006: Robust responses of the hydrological cycle to global warming. *J. Climate,* **19,** 5686–5699.

Jiang, H., and E. Zipser, 2010: Contribution of tropical cyclones to the global precipitation from eight seasons of TRMM data: Regional, seasonal, and interannual variations. *J. Climate,* **23,** 1526–1543.

Knutson, T. R., and S. Manabe, 1995: Time-mean response over the tropical Pacific to increased CO_2 in a coupled ocean–atmosphere model. *J. Climate,* **8,** 2181–2199.

——, and Coauthors, 2010: Tropical cyclones and climate change. *Nat. Geosci.,* **3,** 157–163, doi:10.1038/ngeo779.

Li, T., 2006: Origin of the summertime synoptic-scale wave train in the western north Pacific. *J. Atmos. Sci.,* **63,** 1093–1102.

McDonald, R., D. Bleaken, D. Creswell, V. Pope, and C. Senior, 2005: Tropical storms: Representation and diagnosis in climate models and the impact of climate change. *Climate Dyn.,* **25,** 19–36.

Nolan, D., and E. Rappin, 2008: Increased sensitivity of tropical cyclogenesis to wind shear in higher SST environments. *Geophys. Res. Lett.,* **35,** L14805, doi:10.1029/2008GL034147.

——, ——, and K. Emanuel, 2007: Tropical cyclogenesis sensitivity to environmental parameters in radiative-convective equilibrium. *Quart. J. Roy. Meteor. Soc.,* **133,** 2085–2107.

O'Gorman, P., and T. Schneider, 2008: The hydrological cycle over a wide range of climates simulated with an idealized GCM. *J. Climate,* **21,** 3815–3832.

Randall, D., and Coauthors, 2007: Climate models and their evaluation. *Climate Change 2007: The Physical Science Basis,* S. Solomon et al., Eds., Cambridge University Press, 591–662.

Rotunno, R., and K. Emanuel, 1987: An air–sea interaction theory for tropical cyclones. Part II: Evolutionary study using a nonhydrostatic axisymmetric numerical model. *J. Atmos. Sci.,* **44,** 542–561.

Sugi, M., and J. Yoshimura, 2004: A mechanism of tropical precipitation change due to CO_2 increase. *J. Climate,* **17,** 238–243.

——, A. Noda, and N. Sato, 2002: Influence of the global warming on tropical cyclone climatology: An experiment with the JMA global model. *J. Meteor. Soc. Japan,* **80,** 249–272.

——, H. Murakami, and J. Yoshimura, 2009: A reduction in global tropical cyclone frequency due to global warming. *SOLA,* **5,** 164–167.

Vecchi, G., and B. Soden, 2007: Effect of remote sea surface temperature change on tropical cyclone potential intensity. *Nature,* **450,** 1066–1071, doi:10.1038/nature06423.

Wehner, M., G. Bala, P. Duffy, A. Mirin, and R. Romano, 2010: Towards direct simulation of future tropical cyclone statistics in a high-resolution global atmospheric model. *Adv. Meteor.,* **303,** doi:10.1155/2010/915303.

Yoshimura, J., and M. Sugi, 2005: Tropical cyclone climatology in a high-resolution AGCM—Impacts of SST warming and CO_2 increase. *SOLA,* **1,** 133–136.

——, ——, and A. Noda, 2006: Influence of greenhouse warming on tropical cyclone frequency. *J. Meteor. Soc. Japan,* **84,** 405–428.

Zhao, M., and I. Held, 2010: An analysis of the effect of global warming on the intensity of Atlantic hurricanes using a GCM with statistical refinement. *J. Climate,* **23,** 6382–6393.

——, I. M. Held, S.-J. Lin, and G. A. Vecchi, 2009: Simulations of global hurricane climatology, interannual variability, and response to global warming using a 50-km resolution GCM. *J. Climate,* **22,** 6653–6678.

——, I. Held, and G. Vecchi, 2010: Retrospective forecasts of the hurricane season using a global atmospheric model assuming persistence of SST anomalies. *Mon. Wea. Rev.,* **138,** 3858–3868.